AIAA JOURNAL
Vol. 30, No. 5, May 1992

Prediction and Measurement of Modal Damping Factors for Viscoelastic Space Structures

D. J. McTavish* and P. C. Hughes†
University of Toronto, Downsview, Ontario M3H 5T6, Canada
and
Y. Soucy‡ and W. B. Graham§
Canadian Space Agency, Ottawa, Ontario K2H 8S2, Canada

The procedure outlined in this paper extends the finite element method to viscoelastic space structures; predictions of mode shapes, frequencies, and damping factors can be made based on a new modeling approach that uses specific measured material data. Briefly, the procedure is as follows: 1) the modulus function of the material is measured from free-decay tests of a uniform cantilever beam of the subject material, and 2) these material data are then inserted into the new damped-structure modeling technique. These two steps are illustrated and validated using a strawman space structure fabricated entirely from a single epoxy material. Predicted damping characteristics based on material data and the new modeling technique are compared with modal data obtained for the test structure. Using commercially available software, the modal test data are processed to obtain mode shapes, frequencies, and damping factors. A comparison between predicted eigenvalues and experimentally determined modal frequencies and damping factors indicates that the proposed new technique is a valuable tool in structural analysis.

Introduction

ALTHOUGH energy dissipation is a crucial dynamical characteristic of large space structures, it is usually not well modeled. Material damping has been a subject of interest for decades,[1] yet dynamicists do not have a generally accepted method for modeling the damping characteristics of engineering structures. For large space structures (LSS) in particular, structural damping is an important consideration in actively controlled systems and can be critical in passive systems. LSS are characterized by several key mechanical properties: lightweight (and consequently great flexibility), deployable/retractable, low structural frequencies, relatively dense modal spectrum, and low damping.

Actively controlled space structures are subjected to control forces and torques for stationkeeping, attitude control, shape control, and other requirements of their space mission. The control system is the source of most significant disturbances to the structure. Since control systems are often designed assuming (at worst) no structural damping, or (at best) using modal damping factors that are really only guesses, the control design suffers accordingly. In addition, control system designs for LSS are based on reduced-order models; thus, the natural damping inherent in the unmodeled modes becomes of concern, particularly if some of these modes are excited by the control system.

For these reasons, Golla and Hughes[2] developed an approach to modeling viscoelastic structures that met the following criteria: 1) the approach was to be *predictive* (as distinct from a model for a specific spacecraft based on an isolated set of modal tests), 2) the approach was to be based on a well-defined set of experimental data on the materials from which the structure was composed, and 3) the approach was to be completely compatible with the finite element method (FEM), and thus, must be expressed in linear matrix-second-order form, complete with mass and stiffness matrices. Although the method produced "only" a linear model and did not take into account other sources of energy dissipation (such as joint damping), it represented an important step forward for linear-viscoelastic structures. McTavish extended[3] this approach in several respects: 1) by improving the nomenclature, 2) by designing an appropriate test structure, 3) by creating and carrying out a set of novel material-property experiments, and 4) through other extensions (including light-damping approximations) not discussed herein. This viscoelastic FEM modeling technique will, for brevity, be called the GHM (Golla, Hughes, McTavish)[2,3] method. Validation of this method through material property measurements and full-scale modal testing of the test structure is the subject of this paper.

The work reported in this paper covers the first stage of experimental tests in a collaborative research effort between the University of Toronto Institute for Aerospace Studies (UTIAS) and the Canadian Space Agency (CSA). A brief outline of this work[4] is illustrated in Fig. 1. The project is aimed at addressing the particular shortcomings that exist with respect to the modeling of damping in the dynamics of LSS. The essence of the project is to establish a practical method for modeling damping through a combined theoretical and experimental study. The present work is fundamental and addresses the problem of predicting, from measured material properties, the damping characteristics of an arbitrary lightly damped structure made from a uniform material.

Viscoelastic Finite Element Models

For a linear *elastic* material, the one-dimensional constitutive relation between stress and strain is a simple proportionality with a (constant) elastic modulus: $\sigma(t) = G^e\epsilon(t)$. For a linear *viscoelastic* material, the constant modulus G^e is replaced by a *relaxation function* $G(t)$ within a convolution:

$$\sigma(t) = \int_0^t G(t-\tau)\frac{d\epsilon(\tau)}{d\tau}\,d\tau; \qquad \epsilon(t) \equiv 0, \quad \forall t \le 0 \tag{1}$$

Received Nov. 13, 1990; revision received May 3, 1991; accepted for publication May 13, 1991. Copyright © 1991 by the American Institute of Aeronautics and Astronautics, Inc. All rights reserved.

*Lecturer, Institute for Aerospace Studies, 4925 Dufferin Street. Student Member AIAA.

†Cockburn Professor, Institute for Aerospace Studies, 4925 Dufferin Street. Associate Fellow AIAA.

‡Research Engineer, c/o Communications Research Centre, Box 11490, Station H. Member AIAA.

§Manager, Dynamics Group, c/o Communications Research Centre, Box 11490, Station H.

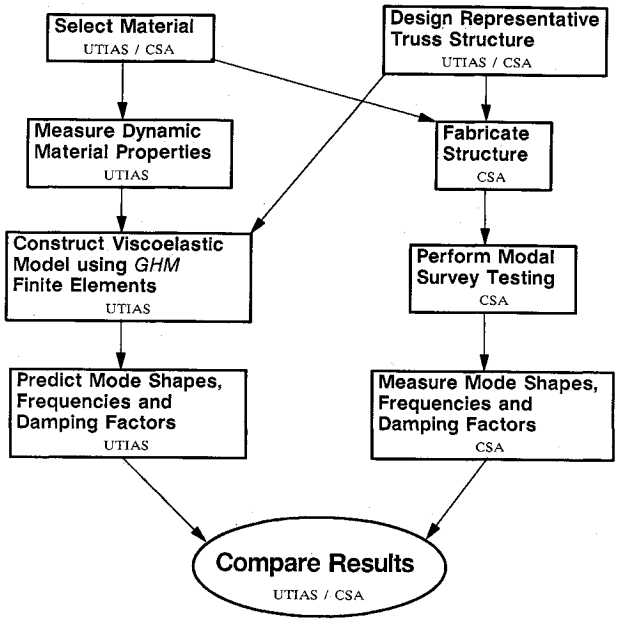

Fig. 1 CSA/UTIAS collaborative damping study.

This is sometimes called a hereditary relationship. Equation (1) can be transformed into the Laplace domain; thus, $\bar{\sigma}(s) = s\tilde{G}(s)\bar{\epsilon}(s)$. We shall call the complex function $s\tilde{G}(s)$ a *modulus function*.

The GHM representation for a modulus function is written as

$$s\tilde{G}(s) \doteq G^e\left[1 + \sum_k \alpha_k \frac{s^2 + 2\hat{\zeta}_k\hat{\omega}_k s}{s^2 + 2\hat{\zeta}_k\hat{\omega}_k s + \hat{\omega}_k^2}\right] \tag{2}$$

The positive constant G^e represents the equilibrium value of the corresponding relaxation function: $G^e = \lim_{t\to\infty} G(t)$. Owing to their second-order form, the rational functions summed in Eq. (2) will be called minioscillator terms. The constants $\alpha_k > 0$, $\hat{\omega}_k > 0$, and $\hat{\zeta}_k > 0$ are determined from test data for the material over the range of s appropriate to the application. An arbitrary number of minioscillator terms may be used to provide more extensive representations of the modulus function.

The GHM method produces a mathematical model of the form

$$\boldsymbol{M}^v\begin{bmatrix}\ddot{\boldsymbol{q}}\\ \dot{\boldsymbol{z}}\end{bmatrix} + \boldsymbol{D}^v\begin{bmatrix}\dot{\boldsymbol{q}}\\ \boldsymbol{z}\end{bmatrix} + \boldsymbol{K}^v\begin{bmatrix}\boldsymbol{q}\\ \boldsymbol{z}\end{bmatrix} = \begin{bmatrix}\boldsymbol{f}\\ \boldsymbol{0}\end{bmatrix} \tag{3}$$

Moreover, $\boldsymbol{M}^v$ is positive definite, $\boldsymbol{D}^v$ is positive semidefinite, and $\boldsymbol{K}^v$ is non-negative definite. For details, see Refs. 2 and 3.

In general, the GHM theory provides for the construction of viscoelastic element matrices where any number of moduli are present and each is representable by an arbitrary number of minioscillator terms. When GHM elements are used in a structural model, they are used exactly as their elastic counterparts. There is no difficulty mixing GHM viscoelastic elements with elastic elements in the same structural model. The element matrices are assembled into the global system with their spatial coordinates overlapping those of neighboring elements at coincident nodes of the structure. There is no overlapping of the dissipation coordinates between elements.

Material Property Measurements

Material data were obtained for the viscoelastic Young's modulus function using the free decay of cantilever beam specimens and noncontact displacement sensing. The free-decay method has the advantage of avoiding the need to implement, calibrate, and monitor a force input to the test item, and noncontact displacement sensing further reduces the intrusion of experimental hardware into the test environment.

To interpret the test results, one needs the equation of motion for a uniform viscoelastic cantilever beam:

$$\rho A\ddot{w}(x,t) + I\int_{-\infty}^{t} E(t-\tau)\frac{\mathrm{d}w''''(x,\tau)}{\mathrm{d}\tau}\,\mathrm{d}\tau = 0 \tag{4}$$

subject to the cantilever boundary conditions $w(0,t) = w'(0,t) = w''(l,t) = w'''(l,t) = 0$. When the motion is represented as a superposition of damped modes,

$$w(x,t) = \sum_i c_i\phi_i(\eta)e^{s_i t}, \quad \eta = x/l \tag{5}$$

it can be shown that the mode shapes obtained are the same as the classical undamped mode shapes:

$$\phi_i(\eta) = (\cosh\beta_i\eta - \cos\beta_i\eta) - \Phi_i(\sinh\beta_i\eta - \sin\beta_i\eta) \tag{6}$$

where, for example, $\beta_1 = 1.875104, \ldots, \Phi_1 = 0.734096, \ldots$, and where the eigenvalues s_i are the solutions of the (complex) characteristic equation

$$s^2 + \bar{\omega}^2 s\bar{E}(s) = 0, \qquad \bar{\omega}^2 = (I/\rho A l^4)\beta^4 \tag{7}$$

The real and imaginary parts of the eigenvalue

$$s = -\delta + j\omega \tag{8}$$

are, respectively, the amplitude decay rate and circular frequency of the motion.

In an ideal free-decay experiment, the eigenvalue s_i of a particular mode is measured. Knowing the dimensions and density of the beam specimen, a point value of the modulus function may be inferred from the characteristic equation (7). The free-decay experiment used was a relatively simple one: clamped at various fixed lengths, the beam specimens were set into motion using a manual hold-and-release technique. This produces primarily the first mode of vibration. The tip displacement throughout the decay was measured using a noncontact sensor described by Greenhow,[5] consisting of a lightweight piece of slide film, developed with a pattern of varying opacity, and attached to the tip of the beam. As the beam moves, the slide film passes freely through the gap of a stationary LED-phototransistor detector to produce a voltage signal. Peak-to-peak displacements of up to 2 cm can be measured with this setup.

Data were acquired and stored using a ZONIC 6088 Signal Processor at preset sampling intervals. During each free-decay run, four contiguous records of 1024 points were stored and then downloaded onto an Apollo computer workstation for voltage-displacement decalibration and further processing; the four 1024-point records were further subdivided into eight subrecords of 512 data points each, as shown in Fig. 2. Several oscillations were captured within each of the subrecords. Typically, an amplitude decay of 4:1 was realized over the eight subrecords. Using a least-squares procedure, a decaying sinusoid was fit to each subrecord. From these eight eigenvalue estimates, an average was taken for the run, and Young's modulus function was calculated at that point. Over the range of amplitude studied, no significant variation in frequency or decay rate was detected from subrecord to subrecord.

By changing the clamped length of the cantilever specimens, eigenvalues and modulus function values were obtained

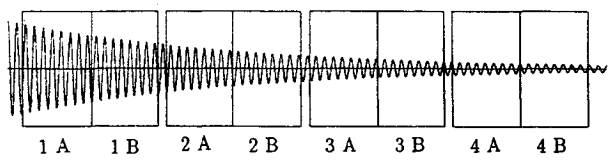

Fig. 2 Data collection strategy (simulated free-decay data).

over a range of frequencies. A set of material data points of the form $\{s,s\tilde{E}(s)\}$ was thereby produced. Three material specimens were used in the testing. Each had a thickness and width of 8.6 and 12.7 mm, respectively. Clamped lengths from between 23 and 70 cm were studied providing free-decay data over a frequency range of 4–40 Hz. Vibration tip amplitudes ranged downward from about 6 mm, with maximum strain levels in the specimens generally not exceeding 250 $\mu\epsilon$. Testing was conducted in air at room temperature with the cantilever specimens arranged to vibrate in a horizontal plane; earlier investigations had uncovered analytically predictable problems with regard to both vertically suspended cantilever specimens (gravity) and thinner specimens (air damping). The present series of tests was designed to minimize these undesirable effects.

In the characteristic equation, Eq. (7), $\bar{\omega}$ depends on the dimensions and density of the beam, and on the mode number, and is constant for any particular free-decay run. This equation predicts that the eigenvalues from a number of free-decay runs should fall along some trajectory through the complex s plane determined by the characteristics of the material modulus function. Figure 3 shows the eigenvalue data from all runs plotted in the s plane. The solid line is the best (logarithmic) fit through the data:

$$y = a + b\Omega, \qquad \Omega = \log\omega, \qquad y = \log\delta \tag{9}$$

where ω and δ are explained in Eq. (8).

A least-squares solution for y and Ω gives $a = -2.341$, $b = 0.9870$. The eigenvalue trajectory can also be written [noting Eq. (8)] as

$$\delta = 0.00456\omega^{0.987} \tag{10}$$

Figures 4 show the modulus function data plotted over the s plane. These data can also be projected along the Ω line, as shown in Fig. 3. Smoothing functions y_1 and y_2 have been fit to the real and imaginary parts of the raw data, as shown by the dashed lines in this figure:

$$y_1(\Omega) = a_1 + b_1\Omega = \log\{\mathrm{Re}\{s\tilde{E}(s)\}_{\mathrm{exp}}\}$$

$$y_2(\Omega) = a_2 + b_2\Omega = \log\{\mathrm{Im}\{s\tilde{E}(s)\}_{\mathrm{exp}}\} \tag{11}$$

with $\{a_1,b_1,a_2,b_2\} = \{9.463,0.00163,7.423,-0.0114\}$. Over the frequency range studied, the Hysol epoxy material evidently has more or less constant real and imaginary parts.

Test Structure Design and Fabrication

A test structure (Fig. 5) was designed to typify the lattice-type construction commonly used in space structures. It consists of two bays, each made up of identical slender beam elements, fabricated so as to ensure that the entire structure behaves as a uniform-material structure. Continuous joints were incorporated using a combination of solid casting and solvent bonding in order to avoid unmodeled joint behavior such as freeplay and friction.

The dimensions of the structure are based on 1) providing ease of handling in the laboratory, 2) having slender but adequately strong beam elements, and 3) possessing a modal spectrum starting at about 5 Hz—a compromise between the desire to emulate the low frequencies characteristic of space structures and the limitations of standard piezoelectric accelerometers. To produce a clean experiment, the structure was designed to maintain well-separated modes (at least amongst the lower modes).

The material used for the structure is Hysol epoxy TE 6175 resin and HD 3561 hardener. When cured, this material is transparent; it exhibits no appreciable shrinkage during or after cure, can be molded easily, and has a desirably low level of material damping. Its mass density is 1176 kg/m^3.

Viscoelastic Finite Element Method Model of the Test Structure

A GHM viscoelastic material model of the experimentally measured Young's modulus function was produced for use in the viscoelastic finite element model. In general, such a representation is based on Eq. (2), with G^e replaced by the (elastic) Young's modulus E^e. Matching a GHM modulus function to given material data can be considered as a curve fitting problem.

For a GHM function with n minioscillator terms, there are potentially $3n + 1$ degrees of freedom. In this study, a three-term model was fit to the material data. To reduce the number of degrees of freedom (from 10 to 6), the three $\hat{\zeta}$ parameters were arbitrarily assigned ($\hat{\zeta}_i = 4$) and the three $\hat{\omega}$ parameters were constrained to form a geometric series. The free GHM parameters were selected through a numerical minimization of the integral

$$I = \int_{\Omega_1}^{\Omega_2} [\{y_1(\Omega) - Y_1(\Omega)\}^2 + \{y_2(\Omega) - Y_2(\Omega)\}^2]\, d\Omega \tag{12}$$

Here, y_1 and y_2 are the logarithms of the real and imaginary

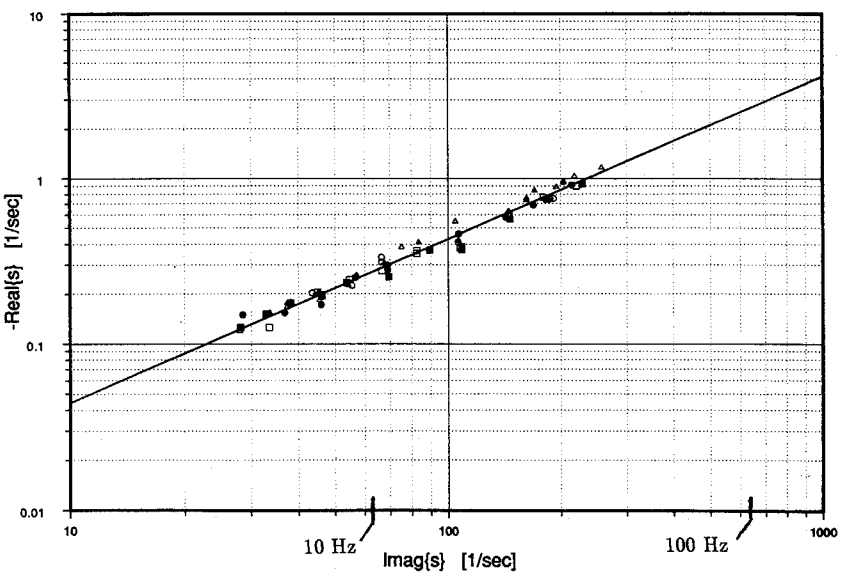

Fig. 3 Free-decay eigenvalue trajectory: the Ω line.

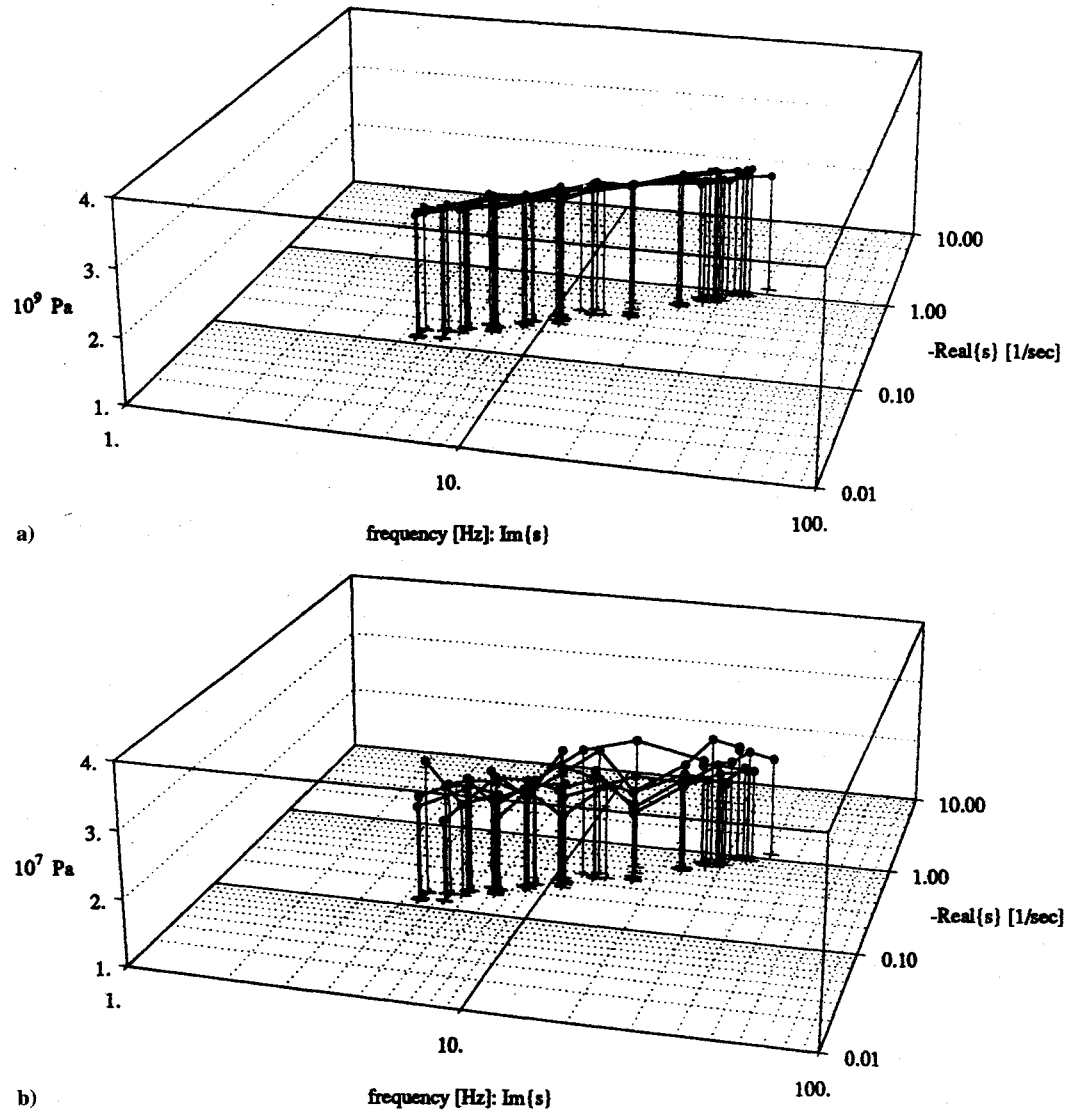

Fig. 4 Measured data for Young's modulus function: a) Young's storage modulus, Re$\{sE(s)\}$; b) Young's loss modulus, Im$\{sE(s)\}$.

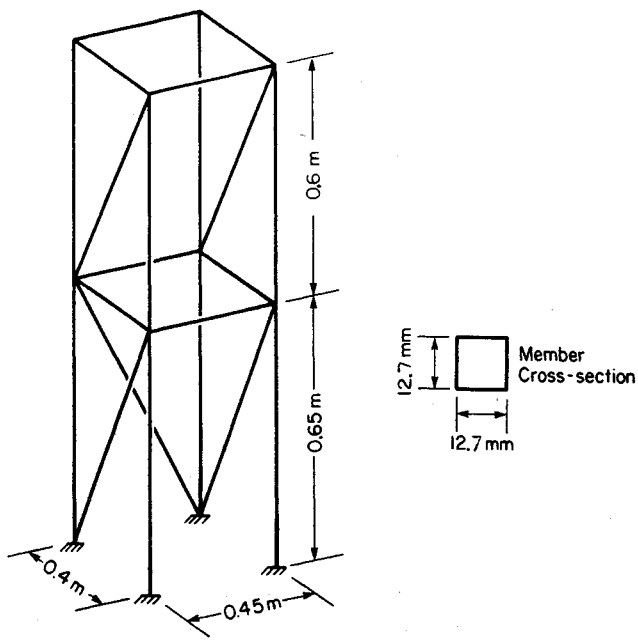

Fig. 5 CSA/UTIAS test structure.

parts of the smoothed experimentally obtained modulus function. Y_1 and Y_2 are the logarithms of the real and imaginary parts of the GHM modulus function expression evaluated along the Ω line:

$$Y_1(\Omega) = \log\{\mathrm{Re}\{s\tilde{E}(s)\}_{\mathrm{GHM}}\}$$

$$Y_2(\Omega) = \log\{\mathrm{Im}\{s\tilde{E}(s)\}_{\mathrm{GHM}}\} \tag{13}$$

$$s = -0.00456(10^{0.987\Omega}) + j10^{\Omega} \tag{14}$$

The limits of the GHM fit were selected to bridge the material data:

$$\Omega_1 = 1.3\ [3.2\ \mathrm{Hz}], \qquad \Omega_2 = 2.6\ [63.7\ \mathrm{Hz}] \tag{15}$$

resulting in the following three minioscillator term model, $E^e = 2.8779$ GPa and

$$\begin{bmatrix}\alpha_1\\ \alpha_2\\ \alpha_3\end{bmatrix} = \begin{bmatrix}0.013005\\ 0.008110\\ 0.012552\end{bmatrix}, \quad \begin{bmatrix}\hat{\omega}_1\\ \hat{\omega}_2\\ \hat{\omega}_3\end{bmatrix} = \begin{bmatrix}130.37\\ 704.40\\ 3805.86\end{bmatrix}$$

$$\begin{bmatrix}\hat{\zeta}_1\\ \hat{\zeta}_2\\ \hat{\zeta}_3\end{bmatrix} = \begin{bmatrix}4.0\\ 4.0\\ 4.0\end{bmatrix} \tag{16}$$

This GHM function is plotted as a solid line in Fig. 6.

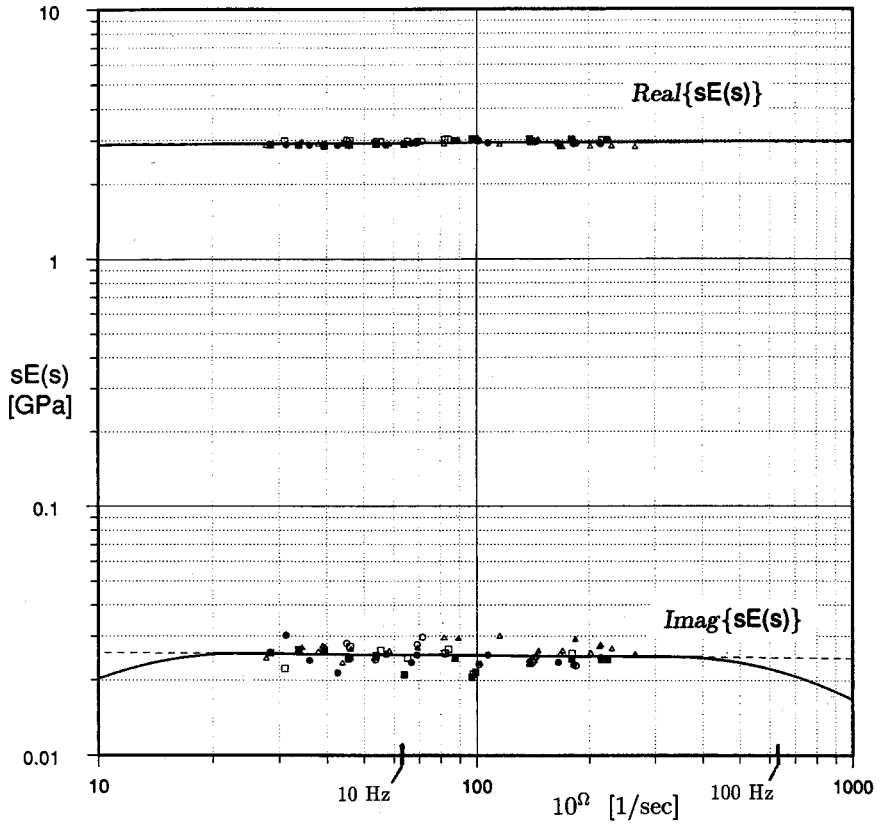

Fig. 6 Three-term GHM modulus function, fit to measured data.

The truss structure is modeled using beam elements, two per member. Since the joints of the structure are continuous, slope continuity is enforced. The elastic mass and stiffness matrices for a beam element in a plane are as follows:

$$\boldsymbol{M} = \boldsymbol{M}_b + \boldsymbol{M}_r \tag{17}$$

$$\boldsymbol{M}_b = \frac{\rho A l}{420}\begin{bmatrix} 156 & 22l & 54 & -13l \\ 22l & 4l^2 & 13l & -3l^2 \\ 54 & 13l & 156 & -22l \\ -13l & -3l^2 & -22l & 4l^2 \end{bmatrix} \tag{18}$$

$$\boldsymbol{M}_r = \frac{\rho I}{30l}\begin{bmatrix} 36 & 3l & -36 & 3l \\ 3l & 4l^2 & -3l & -l^2 \\ -36 & -3l & 36 & -3l \\ 3l & -l^2 & -3l & 4l^2 \end{bmatrix} \tag{19}$$

$$\boldsymbol{K} = \frac{EI}{l^3}\begin{bmatrix} 12 & 6l & -12 & 6l \\ 6l & 4l^2 & -6l & 2l^2 \\ -12 & -6l & 12 & -6l \\ 6l & 2l^2 & -6l & 4l^2 \end{bmatrix} \tag{20}$$

for an element displacement vector $\boldsymbol{q} = \text{col}\{v_1, \theta_1, v_2, \theta_2\}$. Rotary inertia has been included in the mass matrix through $\boldsymbol{M}_r$, whereas shear effects have been neglected throughout.

For a GHM modulus function with three minioscillator terms, the viscoelastic finite element matrices are

$$\boldsymbol{M}^v = \text{diag}\left\{\boldsymbol{M}, \alpha_1 \frac{1}{\hat{\omega}_1^2}\boldsymbol{\Lambda}, \alpha_2 \frac{1}{\hat{\omega}_2^2}\boldsymbol{\Lambda}, \alpha_3 \frac{1}{\hat{\omega}_3^2}\boldsymbol{\Lambda}\right\} \tag{21}$$

$$\boldsymbol{D}^v = \text{diag}\left\{\boldsymbol{O}, \alpha_1 \frac{2\hat{\zeta}_1}{\hat{\omega}_1}\boldsymbol{\Lambda}, \alpha_2 \frac{2\hat{\zeta}_2}{\hat{\omega}_2}\boldsymbol{\Lambda}, \alpha_3 \frac{2\hat{\zeta}_3}{\hat{\omega}_3}\boldsymbol{\Lambda}\right\} \tag{22}$$

$$\boldsymbol{K}^v = \begin{bmatrix} \boldsymbol{K} + (\alpha_1 + \alpha_2 + \alpha_3)\boldsymbol{K} & -\alpha_1\boldsymbol{R} & -\alpha_2\boldsymbol{R} & -\alpha_3\boldsymbol{R} \\ -\alpha_1\boldsymbol{R}^T & \alpha_1\boldsymbol{\Lambda} & \boldsymbol{O} & \text{O} \\ -\alpha_2\boldsymbol{R}^T & \boldsymbol{O} & \alpha_2\boldsymbol{\Lambda} & \text{O} \\ -\alpha_3\boldsymbol{R}^T & \boldsymbol{O} & \boldsymbol{O} & \alpha_3\boldsymbol{\Lambda} \end{bmatrix} \tag{23}$$

where $\boldsymbol{\Lambda} = EI/l^3\ \text{diag}\{2l^2, 12(2 + l^2/2)\}$ and the nonzero elements of $\boldsymbol{R}$ are $r_{21} = -r_{41} = 1/\sqrt{2}$, $r_{12} = -r_{32} = 1/\sqrt{2 + l^2/2}$, and $r_{22} = r_{42} = (l/2)/\sqrt{2 + l^2/2}$. For the three-dimensional beam elements used to model the test structure, bending is included in two orthogonal directions with simple extension and torsion added. Because of limited space, only the planar version of these elements have been displayed here.

Modal Testing of the Structure

In conventional modal testing, the structure under study is attached to a *fixed* base that may be considered rigid. Measured inputs are forces, and measured outputs (responses) are accelerations at selected points on the structure; however, the portable exciter (input device) and associated stinger can affect the estimation of modal damping. To eliminate this source of error, it was decided to test the structure in a *driven*-base configuration, with the (rigid) base driven by an electrodynamic exciter. In this configuration, the input measurement is made with an accelerometer mounted on the moving base and outputs are measured as before. Vigneron and Soucy[6] have shown that modal parameters (frequencies, damping factors, mode shapes) extracted from this driven-base configuration correspond to those in a conventional fixed-base modal test. Moreover, the modal tests were conducted in air since experience in testing similar types of open, truss-like structures indicates no appreciable damping from aerodynamic sources.

The FEM model of the structure had indicated that the first three modes would be well separated (frequencies at about 6, 13, and 19 Hz), that the fourth mode would be fairly isolated near 29 Hz, and that the next seven modes would be clustered in the range 31–34.5 Hz. It was therefore expected that the first three modal damping factors could be estimated quite precisely, that the fourth might still be obtained with some precision, and that higher ones were likely to be only rough estimates. Consequently, the test plan was written mainly for the identification of the first four modes. Furthermore, the FEM model had shown that most of the motion in the first three modes would be the transverse x direction, and for the fourth mode, most would be in the tranverse y direction (with minor x motion). To accommodate the tight test-facility schedule, it was decided to excite only in the x direction.

Figure 7 shows the structure in its test configuration. The structure was mounted to the slip table of a UD 178 kN shaker through an adapter plate. Each of the four columns of the structure was fixed to the plate with a clamping device. To get good mode shapes, 16 accelerometers were mounted on the structure at strategic locations. To reduce the mass loading effect, small accelerometers (3 g each) were used. No accelerometer was mounted in the y direction since four of the first five modes exhibit no motion in this direction. Eight additional accelerometers were mounted on the clamping devices to monitor their motion; these showed that the plate (including the devices) acted in a rigid manner. Finally, an extra accelerometer was mounted at the middle of the plate to serve as a reference. Figure 7 also shows some members of the scaffolding that served to mount the accelerometers on the structure and to support their cables. The scaffolding was erected close to the structure so that the freely hanging portion of the cables was minimal, thus minimizing the damping effect of the cables.

Data were acquired and preprocessed with a commercially available Fourier system configured with 40 A/D channels; hence, the signals of all 25 accelerometers were taken simultaneously. The frequencies of interest ranged from 4 to 36 Hz, encompassing the first 11 modes of the structures (with special interest in the first 4 modes). Because of the low damping of the structure, and in order to increase the accuracy of parameter estimation (especially for damping values), the data were selected to be frequency response functions "zoomed" around each of the first three natural frequencies and around groups of natural frequencies for the higher modes. This meant that the 512 frequency lines were located in a narrow bandwidth ranging from 2.5 to 4.5 Hz. With data zooming, each data acquisition run lasted about 30–45 min.

The first series of runs served to identify the modes (especially natural frequencies and mode shapes) in the frequency range of interest. The response functions associated with the 16 accelerometers mounted on the structure were processed. Parameters were estimated using a complex exponential curve-fitting algorithm due to Leuridan and Vold,[7] commercially available as software (SMAP from LMS). Estimates of the frequencies and damping factors were obtained by curve fitting simultaneously all eight response functions of each run. Finally, the mode shapes were obtained sequentially from these response functions. Figures 8 are examples of an estimated mode shape.

The next set of runs was aimed at investigating the effects of accelerometers and their cables on the measurements. Four successive runs were made with 16, 8, 4, and 1 accelerometers. For the second and subsequent runs, the locations of the remaining accelerometers were chosen to measure the greatest response. The spectral lines were zoomed around the first mode with acquired frequencies ranging from 4 to 8 Hz. The results are shown Table 1. As one can see from the second column, there is a slight increase in the natural frequency as the number of accelerometers is decreased. However, the mass loading effect is almost negligible. On the other hand, the third column shows that the accelerometer cables do have a significant effect on the estimation of damping factors ζ.

To determine ζ as precisely as possible, a second series of runs was carried out with only one accelerometer on the structure. For each mode, the location of this accelerometer was that location (of the original 16) that experienced the greatest motion. These runs were also used to study the sensitivity to the level of excitation level. For the first three modes, estimates of natural frequency and damping were obtained for two different levels of excitation.

For this last series of runs, parameters were estimated using two different software packages in order to cross-check the results of the curve-fitting algorithms. Besides SMAP, the software package MODENT (from Imperial College) was utilized. The advanced circle-fit algorithm of MODENT was ex-

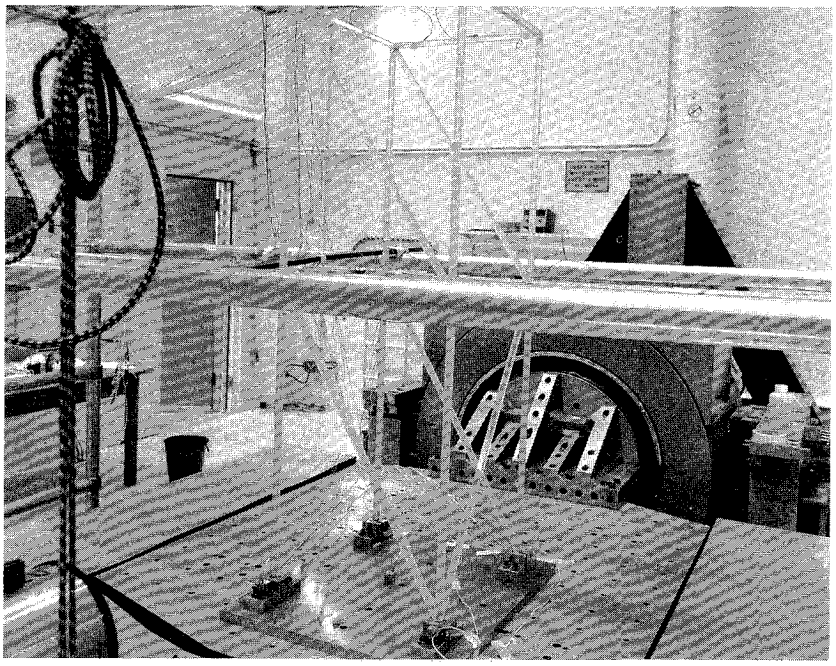

Fig. 7 Modal test setup.

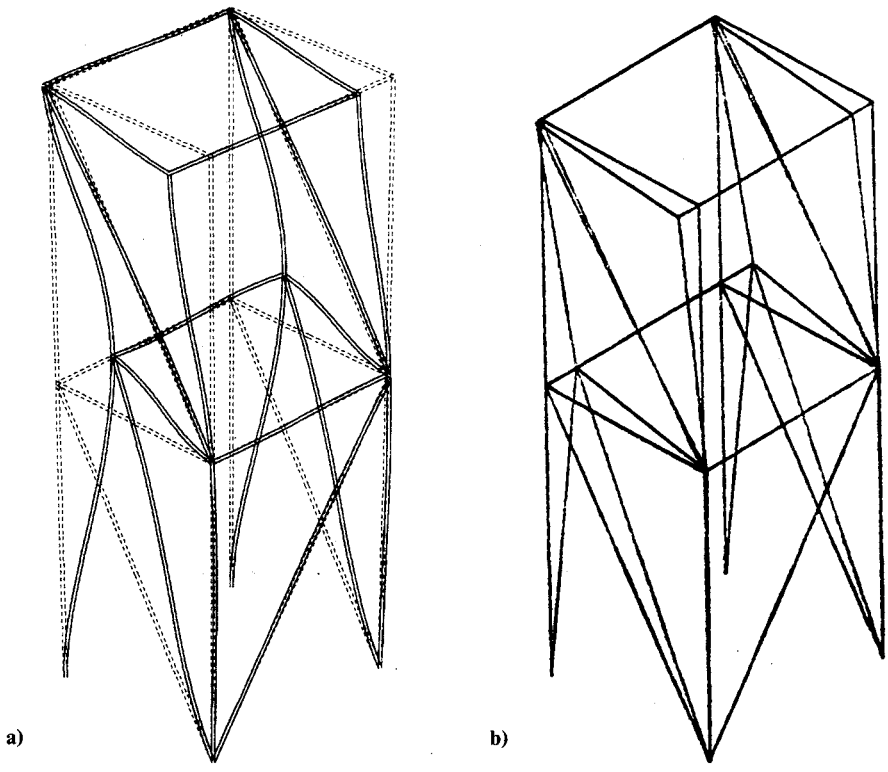

Fig. 8 Second mode shape: a) as predicted from theory; b) as estimated from modal testing.

Table 1 Effects of number of accelerometers

Number of accelerometers	f, Hz	ζ, %
1	6.24	0.38
2	6.21	0.38
8	6.19	0.44
16	6.13	0.52

Table 2 Detailed structural measurements

Mode number	Torque, in.-lb	Excitation level	f, Hz	ζ, % SMAP	ζ, % MODENT
1	10	1	6.24	0.38	0.40
	10	2	6.23	0.37	0.38
	15	1	6.23	0.37	0.37
2	10	1	13.22	0.37	0.36
	10	2	13.23	0.35	0.34
	15	1	13.25	0.35	0.34
3	10	1	19.47	0.35	0.36
	10	2	19.47	0.35	0.34
	15	1	19.65	0.35	0.33
4	10	1	28.71	0.32	0.32
5	10	1	30.67	0.32	0.31
6	10	1	31.79	0.32	0.32
7	10	1	32.18	0.33	0.32
8	10	1	33.01	0.32	0.32
9	10	1	33.34	0.33	0.32
10	10	1	33.84	0.32	0.32
11	10	1	34.45	0.33	0.34

ercised, as well as its SIM option for the fourth and higher closely spaced modes. SIM calculates the contribution from each of the modes previously analyzed and subtracts their contributions from the measured frequency response function data. Used iteratively, SIM permits the data to approach a single-degree-of-freedom pattern.

Table 3 Comparison between predictions and measurements

	GHM finite element prediction			Test results	
Mode	s	f, Hz	ζ, %	f, Hz	ζ, %
1	$-0.1587 + j36.38$	5.79	0.43	6.2	0.38
2	$-0.3323 + j76.94$	12.25	0.43	13.2	0.35
3	$-0.4851 + j113.16$	18.01	0.43	19.4	0.35
4	$-0.7139 + j168.51$	26.82	0.42	28.7	0.32
5	$-0.7589 + j179.30$	28.54	0.42	30.7	0.32
6	$-0.7859 + j185.73$	29.56	0.42	31.8	0.32
7	$-0.8068 + j190.71$	30.35	0.42	32.2	0.32
8	$-0.8155 + j192.77$	30.68	0.42	33.0	0.32
9	$-0.8279 + j195.73$	31.15	0.42	33.3	0.32
10	$-0.8386 + j198.26$	31.55	0.42	33.8	0.32
11	$-0.8494 + j200.82$	31.96	0.42	34.5	0.33

Table 2 presents the estimates of modal frequencies and damping factors. The horizontal lines separating the bandwidths show which modes were identified from the same runs. Column 2 indicates the torque level of the screws in the clamping devices. In column 3, excitation level 1 is about twice as high as excitation level 2. The estimated natural frequencies obtained from SMAP and MODENT are shown in column 4. For the first three modes, the frequency estimates are invariant with respect to the change in the two test parameters.

Estimated damping factors from the two software packages (columns 5 and 6) are generally in excellent agreement, especially if one considers the low level of damping present. For the first three modes, one can see that damping is not really affected by the change in either excitation or torque levels.

Considering the fine agreement between the two damping estimates for modes 6–11, one would consider them as being quite accurate. However, over this frequency range, the relatively small number of accelerometers on the structure (16) makes it very difficult to identify (by comparing mode shapes) which of the analytical modes correspond to the experimental ones.

The predicted and measured modal parameters are summarized and compared in Table 3. Clearly, they correspond

very well, thus validating the approach. As an example of a mode-shape comparison, the second mode is shown in Figs. 8.

Concluding Remarks

This paper has illustrated each step needed to carry out the proposed new approach for predicting damping of viscoelastic structures in practical applications. The GHM method addresses the issue of energy dissipation in structures through the incorporation of linear viscoelastic material properties into the finite element method. It is therefore appropriate for second-order time-domain matrix models and can be used for both steady-state and transient analysis, or with arbitrary input forces as would be needed, for example, in structural control system design. Other sources of damping in structures, notably joint friction, are inherently nonlinear and are not considered here, but could be incorporated into this scheme if available from elsewhere. In general, it can be anticipated that the comprehensive modeling of space structures for which the mechanisms and locations of energy dissipation are important will involve both linear and nonlinear elements.

Acknowledgments

This work was supported by the Canadian Space Agency (Directorate of Space Mechanics) and the Natural Sciences and Engineering Research Council of Canada. The authors are also grateful for the assistance of J. S. Hansen of the University of Toronto Institute for Aerospace Studies with the selection of the material and R. K. Singal of the Canadian Space Agency with the modal tests.

References

[1]Lazan, B. J., *Damping of Materials and Members in Structural Mechanics,* Pergamon, Elmsford, NY, 1968, pp. 35–36.

[2]Golla, D. F., and Hughes, P. C., "Dynamics of Viscoelastic Structures—A Time-Domain Finite Element Formulation," *Journal of Applied Mechanics,* Vol. 52, No. 12, 1985, pp. 897–906.

[3]McTavish, D. J., "The Mini-Oscillator Technique: A Finite Element Method for the Modeling of Linear Viscoelastic Structures," Univ. of Toronto Inst. of Aerospace Studies, Rept. 323, Downsview, Ontario, Canada, May 1988.

[4]Hughes, P. C., McTavish, D. J., Lips, K. W., and Vigneron, F. R., "A New Approach to Modeling Linear Viscoelastic Damping for Space Structures," *Proceedings of the Second Vibration Damping Workshop,* Air Force Wright Aeronautical Labs., AFWAL-TR-86-3059, 1986.

[5]Greenhow, R. C., "Simple Low-Cost Optical Position Transducer," *Journal of Physics E: Scientific Instruments,* Vol. 20, 1987, pp. 602–604.

[6]Vigneron, F. R., and Soucy, Y., "Driven-Base Tests for Modal Parameter Estimation," *AIAA Journal,* Vol. 25, No. 1, 1987, pp. 152–160.

[7]Leuridan, J., and Vold, H., "A Time Domain Linear Modal Estimation Technique for Multiple Input Modal Analysis," *Modal Testing and Modal Refinement,* AMD-Vol. 59, American Society of Mechanical Engineers, New York, 1983, pp. 51–62.